REVISTA MEXICANA DE FÍSICA S **53** (4) 78–93 AGOSTO 2007

Introduction to numerical relativity through examples

F.S. Guzmán
Instituto de Física y Matemáticas, Universidad Michoacana de San Nicolás de Hidalgo,
Edificio C-3, Cd. Universitaria, 58040 Morelia, Michoacán, México,
e-mail: guzman@ifm.umich.mx

Recibido el 1 de mayo de 2006; aceptado el 1 de noviembre de 2006

In these notes some examples of how to apply finite differencing to the solution of partial differential equations are presented and analyzed. The aim of this manuscript is to offer the reader a first step toward the numerical solution of sufficiently complicated and interesting problems within general relativity. The topics include the solution of the wave equation in one spatial dimension and the solution of real and complex self-gravitating scalar fields with spherical symmetry.

Keywords: Numerical methods; numerical relativity; self-gravitating systems.

En estas notas se presentan y analizan algunos ejemplos de aplicación del método de diferencias finitas a la solución de ecuaciones diferenciales parciales. La motivación de este manuscrito es ofrecer al lector un primer paso en la solución numérica de problemas suficientemente complicados e interesantes en relatividad general, o sea, dentro del área llamada relatividad numérica. Los temas incluyen la solución de la ecuación de onda en una dimensión espacial y la solución de campos escalares auto-gravitantes, tanto reales como complejos con simetría esférica.

Descriptores: Métodos numéricos; relatividad numérica; sistemas auto-gravitantes.

PACS: 04.25.Dm

1. Introduction

There is no doubt about the relevance of numerical relativity (NR) in recent years. The most important and urgent application of numerical relativity is the simulation of gravitational wave sources, because the interferometers dedicated to the detection of Gravitational Waves (GWs) are already executing science runs at the threshold of sensitivity. What is needed when filtering the signals measured is a set of confident templates of waveforms associated to certain types of GW sources. One of the most powerful sources of gravitational waves is expected to be the collision of two orbiting black holes; this is the reason why such problem has become the hard core of NR for many years. Currently, the templates used as input for matching the signals in the detectors correspond to postnewtonian approximations of the two body problem for the orbiting stage of the holes, and perturbation theory for the time when the final black hole has been formed. During the last year, striking results indicate that it is possible now to solve numerically the binary black hole problem using full general relativity, and it is possible to estimate the waveforms generated by the system not only during the two stages mentioned above, but also at the merger time [1, 2].

It took a considerable time to design strategies and understand problems in the system of partial differential equations (PDEs) describing the problem of two black holes orbiting around each other. Among the points that favored the recent advances in the solution of this problem within numerical relativity are: the studies on the formulation of the 3+1 decomposition of Einstein's equations and the hyperbolicity properties of its different flavors; the computer power has increased; the algorithms have also evolved and now one accounts with very powerful and accurate algorithms that optimize the resources, *e.g.* the mesh refinement algorithms that optimize the memory to be used in the regions of space with more structure. These are a few items related to the development in the solutions of the PDE system of Einstein's equations, but certainly there are many ways of improving the state of the art within numerical relativity, both, in the branch of numerical algorithms through the introduction of finite element and finite volume methods and in the mathematical sector, where the way the equations are written determines whether or not the system of equations allows a well posed evolution problem.

Aside the hard core of NR there are many other applications that are to come: supernovae core collapse without symmetries, supernova core collapse with neutrino transport, the collapse of a compact star with no symmetries into a black hole, general cases of binary black hole collisions (like unequal mass cases), general relativistic systems in cosmology at high redshift, general relativistic accretion disks and jets. In the field of alternative theories there is a lot to do in tensor-scalar theories, low energy limit of string theory, extended objects like black strings (in fact this is one of the already active topics [3]), bubble space-times [4], etcetera.

Naturally, before attempting the solution of any of those problems it is perhaps useful to analyze simpler cases. In this sense the wave equation in one spatial dimension is the basic problem that exemplifies the process of solving PDEs. I imprint a major effort in the simplest example, that is, the solution of the wave equation in 1+1 dimensions, which is the paradigm of how a system of PDEs has to be solved. With this solution at hand it is possible to find some results in three spatial dimensions with spherical symmetry, a problem that again only involves PDEs with two independent variables.

The goal of this manuscript is not to provide the student a full set of tools to exploit numerical relativity. Instead, the idea is to show a few examples of how to solve the equations of general relativity for some particular systems, and motivate the reader to go beyond the scope of the cases to be mentioned here. In part, the motivation to proceed this way is that it is sometimes convenient to have a simple computational code that works, which is able to reproduce the results in these notes and in classical papers, and afterwards it would be simple to generalize the ideas to more elaborate problems involving general relativity.

Along this manuscript I want to get the reader interested in:

i) topics for which NR is essential,

ii) NR directly through the examples that include a code that works and is able to reproduce the results presented here and in other papers mentioned along the manuscript.

In Sec. 2, the numerical methods related to finite differencing applied to PDE operations are described. In Sec. 3 the solution of the wave equation in one plus one dimensions and details about its general properties are presented. In Sec. 4 a real self-gravitating scalar field is solved, which is nothing but the introduction of self-gravity to a massive Klein-Gordon field. This turns out to be a generalization of the wave equation. In Sec. 5 a further generalization is shown, namely, that of a self-gravitating complex scalar field, and the particular case of boson stars. Finally, in Sec. 6 a few remarks are made and references are suggested.

2. Numerical Methods

2.1. Finite Differences

The item that has to be kept in mind from the beginning, is that when using finite differencing, one is assuming that the domain of the PDEs is discrete. That is, the functions involved in a PDE are evaluated only in a finite number of points. The implication of such restriction is that it is not possible to calculate the solutions with infinite high precision, and there will be always a contribution of a certain error (called discretization error) that contaminates off the continuum problem. Of course, if one thinks on the variety of problems that can be solved numerically that are still unsolved through analytic methods, it seems that the discretization error is a good price to pay.

There are different approximations to the system of equations to be solved, for example, spectral methods assume that the functions involved in the system of differential equations can be expanded as a series of orthogonal functions on a given domain; then orthogonality conditions and recurrence relations are useful to reduce the system to a simpler system of equations for the coefficients of the expansion.

The approximation using finite differencing works in a different way. In order to illustrate how discretization works assume the case of a hypothetical finite domain with a time coordinate t and a spatial coordinate x. Spatial coordinates are defined as a discrete set of points given by $x_j = j\Delta x$ (j integere), and the boundaries correspond to the points x_0 (on the left) and x_N (on the right). Time $t^n = n\Delta t$ (n integere) is also defined only for certain values of the continuum time. Thus a function is defined only for the values for x and t that correspond to points in the mesh in such a way that for a given continuous function f there are available values of it at (t^n, x_j), denoted here by f^n_j. For a uniformly discretized domain, $\Delta x = x_{i+1} - x_i$ and $\Delta t = t^{n+1} - t^n$ indicate the resolution in the spatial and time coordinates respectively.

The finite differencing approximation assumes that the functions involved can be expanded in a Taylor series around every point of the mesh up to a desired order approximation. Therefore, considering the function is defined at the spatial point x_i the value of the function in the nearest neighbors can be calculated as follows:

$$\begin{aligned} f(x_{j-1}) &= f(x_j) - \Delta x f'(x_j) + \frac{\Delta x^2}{2} f''(x_j) \\ &\quad - \frac{\Delta x^3}{6} f''' + O(\Delta x^3) \\ f(x_j) &= f(x_j) \\ f(x_{j+1}) &= f(x_j) + \Delta x f'(x_j) + \frac{\Delta x^2}{2} f''(x_j) \\ &\quad + \frac{\Delta x^3}{6} f''' + O(\Delta x^4) \end{aligned} \quad (1)$$

where the prime denotes derivative with respect to x. Starting from these approximations it is possible to construct difference operators for the derivatives of f^n_i. For instance, by adding the first and the third formulas above one obtains an expression for the first derivative at the point x_j with a second order error

$$f'(x_j) = \frac{f(x_{j+1}) - f(x_{j-1})}{2\Delta x} + O(\Delta x^2);$$

notice that the value of the function at the left and right nearest neighbors is needed in order to calculate this derivative, that is why it is called a centered finite differencing approximation.

In order to obtain the second derivative of f it suffices to write the combination

$$\frac{f(x_{j+1}) - 2f(x_j) + f(x_{j-1})}{\Delta x^2} = f''(x_j) + O(\Delta x^2),$$

which implies the desired expression for the second derivative with second order accuracy as well. As in the previous case, this is also a centered approximation of the second derivative.

In the case of the spatial boundaries, one of the nearest neighbors would be missing, and a centered approximation would require the addition of an extra point (a ghost point)

to the domain; in most problems one prefers to live without ghost points for the purpose of imposing boundary conditions. Therefore one considers that only points to the right in the spatial domain are available (the case of the left boundary), thus one proceeds by writing the approximations of the function considering only points on the right as follows:

$$\begin{aligned} f(x_j) &= f(x_j) \\ f(x_{j+1}) &= f(x_j) + \Delta x f' + \frac{\Delta x^2}{2} f'' + O(\Delta x^3) \\ f(x_{j+2}) &= f(x_j) + 2\Delta x f' + 2\Delta x^2 f'' + O(\Delta x^3). \end{aligned} \quad (2)$$

The combination

$$f(x_{j+2}) - 4f(x_{j+1}) + 3f(x_j) = 2\Delta x f' + O(\Delta x^3)$$

implies the desired expression for the first spatial derivative of the function with second order accuracy; when applied to the left boundary it would read

$$f' = \frac{f(x_2) - 4f(x_1) + 3f(x_0)}{2\Delta x} + O(\Delta x^2).$$

A similar expression can be obtained for the right boundary considering only points on the left.

If one considers now the discretization in time, the operations above apply in the same way and time derivatives are found in a similar way. It is of course possible to construct more accurate approximations to derivatives which would result in better approximations to the continuous equations (see *e.g.* Ref. 5). However more accurate approximations involve points beyond $x_{j\pm1}$ and are unpractical for the purpose of these notes.

On the other hand, when the points in time are considered, it is possible to use the expressions constructed for the calculation of spatial derivatives, for instance, the first time derivative at time t^n is approximated to second order by

$$\frac{\partial f}{\partial t} = \frac{f_j^{n+1} - f_j^{n-1}}{\Delta t} + O(\Delta t^2).$$

The second derivative calculated to second order centered at time t^n reads

$$\frac{\partial^2 f}{\partial t^2} \rightarrow \frac{f_i^{n+1} - 2f_i^n + f_i^{n-1}}{(\Delta t)^2} + O(\Delta t^2).$$

With the operators for the second derivatives it is easy to construct the discretized version of the wave equation

$$\frac{\partial^2 f}{\partial t^2} - \frac{\partial^2 f}{\partial x^2} = 0$$

centered at the point (t^n, x_i):

$$\frac{f_i^{n+1} - 2f_i^n + f_i^{n-1}}{(\Delta t)^2} = \frac{f_{i+1}^n - 2f_i^n + f_{i-1}^n}{(\Delta x)^2} + O(\Delta x^2, \Delta t^2) \quad (3)$$

for every i and n. From this expression it is possible to solve for f_i^{n+1}, and provided values of the function f at the time labels n and $n-1$ it is possible to calculate the values of f at the label $n+1$. This is an example of how, given initial conditions, the solution for further times can be constructed. An important note about finite differences is that because the approximations of the differential operators involved in the PDEs are obtained through a Taylor series expansion, an error in the definition of the differential equations is introduced due to the truncation of the Taylor series up to a given order. In fact, it is expected that the error term in (3) decreases when increasing the resolution in time and space.

In what follows the equations one deals with are discretized in a similar manner in order to construct a global solution for a given set of PDEs in terms of initial conditions.

2.2. Convergence

As mentioned above, when solving equations using finite differencing one is discretizing the equation, and therefore the equations whose solution is being calculated are not exactly those assumed to be valid in the continuum, a truncation error in the Taylor series expansion is being introduced through the simple fact of discretizing. Moreover, even though the error involved in the discretized version of an equation decreases when increasing the resolution, it is necessary to establish at what rate such error should decrease. The convergence is the notion that relates the rate at which the error decreases in terms of the accuracy of the discretization. However there is a concept in between, that of consistency: it is said that a discretization is consistent given that for smaller values of Δx and Δt the error with respect to the solution in the continuum decreases. Another concept is that of stability, which is a measure of the increase rate of the values of the function one is calculating; for instance in (3) if one chooses resolutions such that $\Delta t/\Delta x > 1$ it is clear that the amplitude of the wave function will increase after every time iteration, until it gets out of control. This is only one case, but in general the stability is related to the time integration algorithm like those used later on in these notes. If the two conditions, stability and consistency are satisfied, it is said that the algorithm converges. This is known as the Lax theorem. In order to illustrate what convergence means and how one can see whether the calculations provide convergent results I follow the notes in Ref. 6.

Consider a function f_j that is second order accurate (like the operators described above) such that

$$f(x) = f_0(x) + E(x)(\Delta x^2) + O(\Delta x^3),$$

where $f_0(x)$ is the exact solution at the continuum, E denotes the unknown error term. If $f_0(x)$ is known, it is enough to compare the results obtained with two different resolutions f_1 obtained using Δx and f_2 obtained using $\Delta x/2$. Then the theory predicts that

$$\frac{f_1 - f_0}{f_2 - f_0} = \frac{\Delta x^2 + O(\Delta x^3)}{\frac{1}{4}\Delta x^2 + O(\Delta x^3)} = 4 + O(\Delta x^3). \quad (4)$$

For instance, for the wave equation (3) one knows the analytic solution, and it would be a matter of using two different resolutions to verify whether the difference between the exact and numerical solutions converges to zero. A different story happens when the exact solution is unknown; however, within general relativity, even though the solution might be unknown, in the 3+1 decomposition the system of PDEs is overdetermined, that is, there are evolution equations for the dynamical variables (the number of this variables depends on the formulation and the gauge one chooses, ADM and BSSN are the most common ones, see *e.g.* Ref. 7) and there are also constraint equations that are to be satisfied. The Hamiltonian and momentum constraints (say $H = 0$ and $M^k = 0$) are assumed to be satisfied during the evolution; nevertheless the truncation error introduced when the equations are discretized imply that these constraints are not exactly satisfied. The advantage is that one knows they have to be satisfied (*e.g.* $H = 0$) in the continuum limit; therefore only two resolutions suffice to verify whether the calculations are correct.

In the most general case, when the exact solution is unknown, one can do a Cauchy-type convergence test, using the results with three different resolutions. Say f_1 and f_2 as above, and furthermore f_4 which has been computed using $\Delta x/4$, then

$$\frac{f_1 - f_2}{f_2 - f_4} = \frac{\Delta x^2 - \frac{1}{4}\Delta x^2 + O(\Delta x^3)}{\frac{1}{4}\Delta x^2 - \frac{1}{16}\Delta x^2 + O(\Delta x^3)} = \frac{\Delta x^2 + O(\Delta x^3)}{\frac{1}{4}\Delta x^2 + O(\Delta x^3)} = 4 + O(\Delta x^3). \quad (5)$$

This type of estimates provide indications of a good or a bad calculation. For instance, if one finds that the convergence factors above (the number 4) happens to be a smaller number, then one has to accept that the convergence of the solution is not as good as expected. The possible reasons for such a situation are: there is an error in the implementation of the algorithm or the algorithm itself does not converge in the range of Δx selected.

3. The wave equation in 1+1

The wave equation appears as a work horse example to illustrate how finite differencing is applied to a concrete problem. With this example, I will also introduce the notion of a space+time decomposition. In this sense, I call to concepts defined in the 3+1 decomposition of space-time in general relativity, in particular the concepts of "lapse function" and "shift vector". Thus one has the chance to learn also a little bit of how gauge freedom works and how one can take advantage of such gauge freedom. This section is a generalization inspired in a previous set of notes devoted to the wave equation [8].

Now it is shown how the lapse and shift work together to actually control the evolution of initial data according to the wave equation in 1+1 dimensions, which on the other hand is a good introduction to the equations used in full 3+1 general relativity. For this, it is necessary to write down the flat space-time metric in 1+1 dimensions $ds^2 = -d\tilde{t}^2 + d\tilde{x}^2$, which under the general coordinate transformation $dt = \alpha d\tilde{t}$ and $dx = d\tilde{x} - \beta d\tilde{t}$ reads

$$g_{\mu\nu} = \begin{pmatrix} (-\alpha^2 + \beta^2) & \beta \\ \beta & 1 \end{pmatrix}, \quad (6)$$

$$g^{\mu\nu} = \begin{pmatrix} -1/\alpha^2 & \beta/\alpha^2 \\ \beta/\alpha^2 & (1 - \beta^2/\alpha^2) \end{pmatrix}. \quad (7)$$

where $\alpha > 0$ is the lapse function and β is the shift vector, in this case with only one component. Notice that $\mu, \nu = t, x$. In general, the D'Alambertian operator for a given space-time metric is defined as

$$\Box\phi = \frac{1}{\sqrt{-g}}\partial_\mu[\sqrt{-g}g^{\mu\nu}\partial_\nu\phi].$$

From (6) $\sqrt{-g} = \alpha$. The wave equation written in such form can be expanded as follows

$$\begin{aligned} 0 &= \Box\phi \\ &= \frac{1}{\sqrt{-g}}\partial_\mu[\sqrt{-g}g^{\mu\nu}\partial_\nu\phi] \\ &= \frac{1}{\alpha}\partial_t[\alpha g^{t\nu}\partial_\nu\phi] + \frac{1}{\alpha}\partial_x[\alpha g^{x\nu}\partial_\nu\phi] \\ &= \frac{1}{\alpha}\partial_t[\alpha g^{tt}\partial_t\phi + \alpha g^{tx}\partial_x\phi] + \frac{1}{\alpha}\partial_x[\alpha g^{xt}\partial_t\phi + \alpha g^{xx}\partial_x\phi] \\ &= \frac{1}{\alpha}\partial_t\left[-\frac{1}{\alpha}\partial_t\phi + \frac{\beta}{\alpha}\partial_x\phi\right] \\ &+ \frac{1}{\alpha}\partial_x\left[\frac{\beta}{\alpha}\partial_t\phi + \alpha\left(1 - \frac{\beta^2}{\alpha^2}\right)\partial_x\phi\right]. \end{aligned} \quad (8)$$

As will be seen later on, it is desirable to write down a PDE as a system of equations with only first order derivatives in space and time. The reason for this is that it becomes simpler to study the properties of the system of equations (*e.g.* whether it is hyperbolic or not).

The expression above suggests the definition of two new variables $\psi := \partial_x\phi$ and $\pi := (\partial_t\phi - \beta\partial_x\phi)/\alpha$. Notice that π is the argument of the first order time derivative in (8). The idea is to separate such equation into a system of equations for these new variables. The first equation is evident from (8):

$$\partial_t\pi = \partial_x(\alpha\psi + \beta\pi). \quad (9)$$

If now one assumes ϕ is at least continuously twice differentiable, the equation for ψ is $\partial_t\psi = \partial_x(\partial_t\phi)$ which means

$$\partial_t\psi = \partial_x(\alpha\pi + \beta\psi). \quad (10)$$

Equations (9)-(10) are the first order version of the wave equation. This reminds us that the original unknown function is ϕ, which can be recovered using the definition of π once π and ψ have been calculated, that is $\partial_t\phi = \alpha\pi + \beta\psi$.

3.1. Characteristic analysis

If one defines a state vector by $\mathbf{u} = (\pi, \psi)^T$ it is possible to write the wave equation (9)-(10) as

$$\partial_t \mathbf{u} + \mathbf{A}\partial_x \mathbf{u} = -\partial_x(\mathbf{A})\mathbf{u}, \tag{11}$$

where

$$\mathbf{A} = -\begin{pmatrix} \beta & \alpha \\ \alpha & \beta \end{pmatrix}. \tag{12}$$

The characteristic directions, that is, the local directions of propagation of signals in the tx-plane can be found by calculating the eigenvalues of $\mathbf{A}$ (notice that the important $\mathbf{A}$ in the characteristic analysis is the one on the left hand side, where the advection terms reside), thus one solves the equation $\det(\mathbf{A} - I_2\lambda) = 0$ for $\lambda = dx/dt$, where I_2 is the 2×2 identity matrix. The result is as follows

$$\lambda_\pm = -\beta \pm \alpha. \tag{13}$$

Given the two eigenvalues are distinct and real, the system is strictly hyperbolic (a common reference about the hyperbolicity properties of a system of equations is Ref. 9). In the case $\beta = 0$ and $\alpha = 1$ the usual light-cone $x = x_0 \pm t$ is obtained, which determines the local domain of dependence and influence of the fields propagating through the point x_0.

The corresponding eigenvectors for $\lambda_\pm$ are $u_1 = (1, -1)^T$ and $u_2 = (1, 1)^T$. The matrix that diagonalizes $\mathbf{A}$ is therefore

$$\mathbf{P} = \begin{pmatrix} 1 & 1 \\ -1 & 1 \end{pmatrix}, \quad \mathbf{P}^{-1} = \frac{1}{2}\begin{pmatrix} 1 & -1 \\ 1 & 1 \end{pmatrix} \tag{14}$$

From here, $\mathbf{A}$ can be written as $\mathbf{A} = \mathbf{P\Lambda P^{-1}}$ with $\mathbf{\Lambda} = diag(\lambda_+, \lambda_-)$. Multiplying equation (11) by $\mathbf{P}^{-1}$ one finds

$$\begin{aligned} \mathbf{P}^{-1}\partial_t \mathbf{u} + \mathbf{P}^{-1}\mathbf{A}\partial_x \mathbf{u} &= -\partial_x(\mathbf{P}^{-1}\mathbf{A})\mathbf{u} \\ \partial_t \mathbf{w} + \mathbf{\Lambda}\partial_x \mathbf{w} &= -\partial_x(\mathbf{\Lambda})\mathbf{w}, \end{aligned} \tag{15}$$

where

$$\mathbf{w} = \mathbf{P}^{-1}\mathbf{u} = \frac{1}{2}(\pi - \psi, \pi + \psi)^T = (R, L)^T \tag{16}$$

are the characteristic variables. In this way, the two equations (9) and (10) decouple, and the dynamics of the scalar field has been decomposed into a mode moving to the right $[R = 1/2(\pi - \psi)]$ and another moving to the left $[L = 1/2(\pi + \psi)]$. Equation (15) is thus a decoupled pair of advection equations for these new variables R and L.

3.2. Initial data

In the first order form of the wave equation, what is needed at the initial time is the value of $\pi(0, x)$ and $\psi(0, x)$. This is equivalent to providing data for ϕ and its time derivative. In order to focus on the evolution of the initial data one may simply choose time-symmetric initial data for a gaussian profile:

$$\begin{aligned} &\phi(0, x) = Ae^{-(x-x_0)^2/\sigma^2} \Rightarrow \\ &\psi(0, x) = -2\frac{(x - x_0)}{\sigma^2}\phi(0, x) \\ &\pi(0, x) = 0. \end{aligned} \tag{17}$$

It is well known that the solution to the wave equation is the superposition of one mode moving to the right and one mode moving to the left ($\phi(t, x) = f(x + t) + g(x - t)$). Then, the evolution of the initial data above should show the decomposition of the initial data into two gaussians.

3.3. Evolving data

The evolution of data consists in calculating the function f_j^{n+1} from data in the previous time slice. In order to illustrate this fact, discretize equation (9) with $\beta = 0$ and $\alpha = 1$. In this particular case, the discretization at the point (t^n, x_i) reads

$$\begin{aligned} \frac{\pi_i^{n+1} - \pi_i^n}{\Delta t} &\approx \frac{\psi_{i+1}^n - \psi_{i-1}^n}{2\Delta x} \Rightarrow \\ \pi_i^{n+1} &= \pi_i^n + \frac{\Delta t}{2\Delta x}(\psi_{i+1}^n - \psi_{i-1}^n), \end{aligned} \tag{18}$$

where the results of finite differencing above have been used assuming Δt and Δx are small. A similar expression is found for the evolution of ψ from (10). In order to know the value $\pi(t^{n+1}, x_i)$ one must know the values of ψ in the neighboring points (t^n, x_{i+1}), (t^n, x_{i-1}) and the value of π at (t^n, x_i). Such discretization is known as forward in time and centered in space (FTCS); the molecule used to construct data in the $n + 1$ slice is shown in Fig. 1. It is a simple discretization and easy to implement, however it is unstable. Nevertheless, the discretization in this example illustrates how a powerful approach works: the method of lines. Within this approach, it is assumed that for each i the PDE satisfies an ordinary differential equation (ODE) along the vertical lines in Fig. 1. With this in mind, it suffices to have the discretization provided by (18) and integrate in time the resulting differential equation for $\partial_t \pi$. The terms other that the time derivative of the PDE are considered to belong to the right hand side of the ODE in time. Thus only an ODE integrator is required to evolve the data from one time slice to the next one. One only needs to choose the integrator, which is selected according to the accuracy, the dissipation and the stability properties that depend on the restrictions on the Courant factor $\Delta t/\Delta x$ (To learn about the properties of evolution algorithms I refer the reader to references [9–11]). In the present notes the third order Runge-Kutta algorithm is the one used for the evolution of the different systems. A simplified illustration of this algorithm assumes the unknown function f to be such that $\partial_t f = S$ where S would be, for instance, the right hand side

(RHS), then the algorithm to calculate f^{n+1} in terms of information on the previous time slice is

$$f^* = f^n + \Delta t S^n$$
$$f^{**} = \frac{3}{4}f^n + \frac{1}{4}f^* + \frac{\Delta t}{4}S^*$$
$$f^{n+1} = \frac{1}{3}f^n + \frac{2}{3}f^{**} + \frac{2}{3}\Delta t S^{**}.$$

This algorithm is widely used because it requires only three iterations and is accurate and stable for small values of the Courant factor.

3.4. Boundary conditions

As can be seen from Eq. (18) and Fig. 1, the value of the variable to be updated can be calculated only in the interior points, not those located at the boundaries: x_0, x_N; the reason is that here is a spatial derivative on the right hand side of the evolution equation for π. This is not an obstacle but an opportunity to impose boundary conditions over the desired functions at those points. The case of the 1+1 wave equation is the simplest case, and it is possible to impose different types of boundary conditions:

i) periodic, which assume a change of topology of the domain and glue one end of the spatial domain to the other one;

ii) reflecting, which reflects the wave once it reaches the boundary points and

iii) Sommerfeld or outgoing wave, which absorbs the wave.

Because most of the systems related to general relativity are assumed to be isolated systems, and because the spatial domain used to solve the PDEs is usually finite, in the examples shown below the later condition is used.

In other words, the condition on the left boundary is the elimination of the mode that travels to the right ($R = 0$) which means that one does not allow reflections from the left boundary, and the condition on the right boundary is to eliminate the mode traveling to the left ($L = 0$). Explicitly, on the left boundary x_0 one demands

$$\frac{1}{2}(\pi_0^n + \psi_0^n) = L_0$$
$$\frac{1}{2}(\pi_0^n - \psi_0^n) = R_0 = 0, \qquad (19)$$

with solution $\pi_0^n = \psi_0^n = L$. Equivalently, the condition on the right boundary would be $\pi_N^n = R_N$ and $\psi_N^n = -R_N$. The problem reduces to calculate L_0, R_0, L_N and R_N.

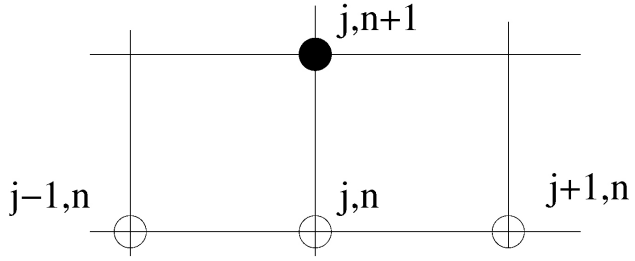

FIGURE 1. Illustration of the molecule used to construct the solution at the $n+1$ time slice. A filled circle indicates the place where one wants to know the desired variable onto, and with empty circles the location where the functions involved are known.

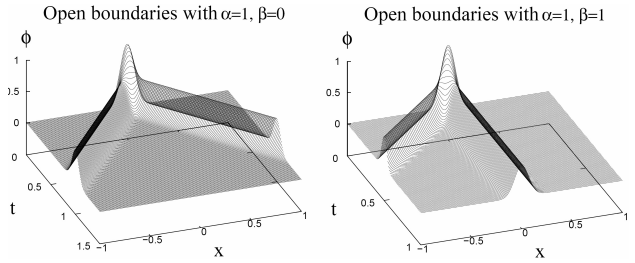

FIGURE 2. Two solutions of the wave equation with outgoing wave boundary conditions are shown. (Left) The usual wave equation; the initial gaussian splits into two smaller gaussians which travel towards the boundaries. (Right) The wave equation with $\beta = 1$ which implies that our coordinates are surfing on top of one of the small gaussians. That is, the coordinates used travel at the speed of the wave ($c = 1$).

3.5. Results

With all these concepts in mind, that is: initial data, an algorithm to evolve functions from one time slice to the next one, boundary conditions and a code that contains all these ingredients together, one can construct several solutions to the wave equation. Here, only a few illustrative ones are presented. The spatial domain used is $-1 \leq x \leq 1$ with resolution $\Delta x = 0.002$ and $\Delta t = 0.0005$.

In Fig. 2 two cases with unit lapse are shown. In the first case $\beta = 0$, which corresponds to the usual wave equation. In fact, it can be seen that the initial gaussian splits into the two expected pulses that reach the boundaries at the same time (around $t \sim 1$). However, in the second case $\beta = 1$, that is, the coordinates are moving toward $x > 0$ at the speed of the propagation of the wave; thus the coordinate system is chasing one of the pulses, which appears in the plot as centered at $x = 0$; the other pulse reaches the boundary in half the coordinate time, which indicates that it is moving twice as fast in the coordinates used.

An example that illustrates the role of the lapse α is the one shown in Fig. 3. In such case a smooth version of a step function is chosen for the lapse, bringing it from the value 0.5 to 1.0. The effect is that being α^2 the coefficient of dt^2 determines how separated the space-like slices are. Therefore, the evolution in the region with $\alpha = 0.5$ ($x < 0$) is slower than in the region with $\alpha = 1$ ($x > 0$). In fact, in the former

case it takes the pulse twice a long ~ 2 to reach the boundary whereas in the latter case the pulse reaches the boundary in regular time ~ 1. This type of behavior is very useful in general relativistic scenarios. For instance, when a black hole is formed as a result of the collapse of a star, what is found is that the geometric invariants start diverging near the center of the system, and therefore one possibility to elude this problem is to choose a slicing condition that squeezes the slices in this region by demanding $\alpha \to 0$ in this region, so that the evolution tends to freeze out.

As a final example, in Fig. 4 a solution with $\alpha = 1$ and $\beta = x$ is shown. Notice that the coordinates travel at the speed of the wave on the boundaries because there, $\beta = \pm 1$. This implies that the signals will never reach the numerical boundaries. The effect is that the pulses in these coordinates squeeze as they approach the boundaries. On one hand this is an advantage, because one does not need to impose boundary conditions (the signals will never reach the boundary), but on the other hand, the pulse is being resolved with less and less points from the domain, which affects the accuracy of the calculations. Anyhow, this example illustrates what can be done with the smart election of a shift condition.

4. Self-gravitating scalar field

An interesting ingredient that can be added to the previous case is gravity. The simplest generalization of the wave equation toward general relativity is to consider that the wave function is associated to a scalar field, which furthermore has

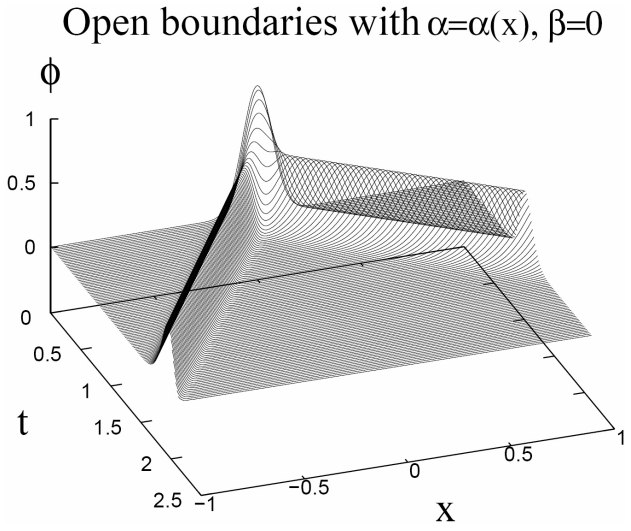

FIGURE 3. The wave equation with β=0 and α=$0.25\tanh(10x) + 0.75$ which is a smooth version of a step function jumping from 0.5 to 1.0. It can be observed that in the region where $\alpha = 0.5$ ($x < 0$), the wave propagates with a slow speed in these coordinates (it can be seen that the signal reaches the boundary after the other pulse). This is so because one has used a foliation with time interval $0.5dt$ where the time slices are closer together than in the region with $x > 0$, for which the time interval is $1.0dt$.

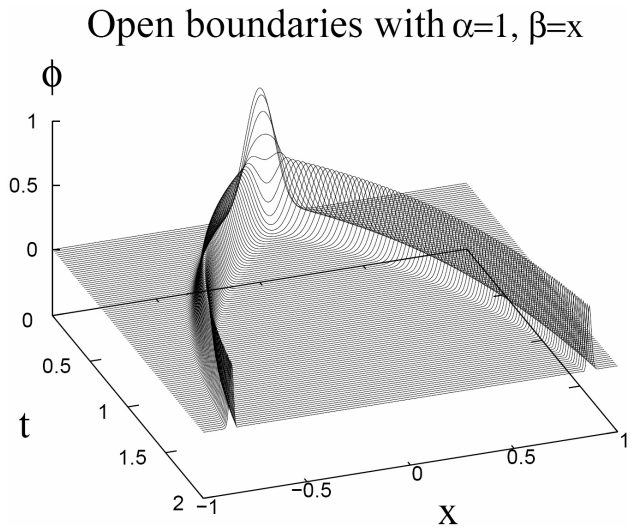

FIGURE 4. The wave equation with $\beta = x$ and $\alpha = 1$. Because the shift equals the speed of propagation of the wave of the boundaries, the signals will never reach the boundaries. The gaussians squeeze as they approach the boundaries because in those regions the coordinates travel at the speed of propagation of the wave.

a stress energy tensor associated to it. In these notes I go one step further, the Klein-Gordon equation which is a generalization of the wave equation with a mass term on it. Of course, this set up has different angles of analysis and a reference that analyzes the system starting from the lagrangian density is [12], which also contains several features, some of which are to be studied in these notes. Here it suffices to mention that the stress energy tensor for such a scalar field reads:

$$T_{\mu\nu} = \phi_{,\mu}\phi_{,\nu} - \frac{1}{2} g_{\mu\nu} \left[\phi^{,\alpha}\phi_{,\alpha} + 2V(\phi)\right] \qquad (20)$$

which is connected to the space-time geometry through Einstein's equations $G_{\mu\nu} = \kappa_0 T_{\mu\nu}$ where $\kappa_0 = 8\pi G$ in units where $c = 1$; $V(\phi)$ is the scalar field potential, which will be considered here to be of the form $\frac{1}{2}m^2\phi^2$, where m is interpreted in field theory as the mass of a spinless boson represented by the scalar field. For simplicity, from now spherical symmetry is assumed. An important restriction about solutions to Einstein's equations coupled to a non-trivial real scalar field in spherical symmetry, is that it is not simple to construct solutions that are assymptotically Schwarzschild with non-trivial scalar field, and many subtleties have to be considered for their existence, like the shape and sign of the scalar field potential. A way around is to assume the space-time to be time-dependent. The price to pay is that the equations describing the system become a PDE system with one spatial and one time coordinates. Under such assumption it is possible to write the line element in Schwarzschild coordinates as

$$ds^2 = -\alpha^2(r,t)dt^2 + a^2(r,t)dr^2 + r^2 d\Omega^2, \qquad (21)$$

where α is the lapse function in the 3+1 decomposition and where $\beta^r = 0$ is assumed. Here r and t are the radial and

time coordinates respectively, which were chosen this way because they are the most common in basic texts in general relativity. In order to remove some constants from Einstein's and Klein-Gordon equations, it is possible to use the scaled variables $\phi \to \sqrt{\kappa_0}\phi$, $r \to mr$ and $t \to mt$. The Bianchi identity for the stress-energy tensor above implies the aforementioned Klein-Gordon equation:

$$\Box\phi - \phi = 0, \tag{22}$$

where, as before

$$\Box\phi = \frac{1}{\sqrt{-g}}\partial_\mu[\sqrt{-g}g^{\mu\nu}\partial_\nu\phi],$$

and where $\phi = \phi(r,t)$. Observe that the rescaling of the variables remove the presence of the constants in Einstein's equations and the scalar field mass. Notice that here g and $g^{\mu\nu}$ this are the determinant of the metric and the inverse metric calculated from (21). Notice also that because ϕ is time dependent in general, the metric might also be time-dependent. In order to take advantage of the tools developed in the previous section, one defines first order variables. In fact, after developing the D'Alambertian as done in Eq. (8) one realizes that a good set of first order variables is given by $\psi = \partial_r\phi$ and $\pi = a\partial_t\phi/\alpha$. Considering these new variables, Einstein's equations read

$$\frac{\partial_r a}{a} = \frac{1-a^2}{2r} + \frac{r}{4}\left[\psi^2 + \pi^2 + 2a^2V\right], \tag{23}$$

$$\frac{\partial_r \alpha}{\alpha} = \frac{\partial_r a}{a} + \frac{a^2-1}{r} - ra^2V, \tag{24}$$

$$\partial_t a = \frac{1}{2}r\alpha\phi\pi, \tag{25}$$

where Eq. (23) is the Hamiltonian constraint, (24) is the (r,r) component of Einstein's equations, which is also the condition that guarantees that r remains the radial areal coordinate, and (25) is the momentum constraint. This set of equations is overdetermined and one has to choose which of the equations are to be solved. As in Ref. 12, the first two equations are used and the momentum constraint is used only for monitoring the accuracy and convergence of the calculations.

On the other hand, the Klein-Gordon equation is written as a set of three equations (see (9) and (10) for comparison):

$$\partial_t\phi = \frac{\alpha}{a}\pi, \tag{26}$$

$$\partial_t\pi = \frac{1}{r^2}\partial_r\left(\frac{r^2\alpha\psi}{a}\right) - a\alpha\phi, \tag{27}$$

$$\partial_t\psi = \partial_r\left(\frac{\alpha\pi}{a}\right), \tag{28}$$

which completes the set of PDEs describing a self-gravitating real scalar field. The question is what to do with Eq. (25). In fact one assumes that if the rest of the equations are being solved exactly, this constraint has to be satisfied. However one cannot be sure of that because -as pointed out in Sec. 2.2.- it can be satisfied only up to the truncation error. Therefore, one can only verify whether or not this equation is satisfied in the continuum limit, that is, verify that the quantity $\partial_t a - \frac{1}{2}r\alpha\phi\pi$ converges to zero in the continuum limit.

One important detail in Eq. (27) is that the first term is singular for $r = 0$. Two things apply: i) a usual procedure is to avoid the origin and stagger the grid, which will be defined now starting from $-dr/2$ on, ii) even though, the differential operator would not converge at the origin. This problem is addressed by using the expression

$$3\frac{d}{dr^3}\left(\frac{r^2\alpha\psi}{a}\right)$$

for the first term in (27), where the d/dr^3 indicates derivation with respect to r^3. This is a common practice in spherically symmetric codes (see *e.g.* Refs. 12 and 13) and is used to obtain the results presented in these notes.

4.1. Initial data

In this case, initial data must satisfy certain equation, namely the set (23-25) and is not as simple as placing a gaussian and evolve it as for the wave equation. In general, in the 3+1 decomposition one has to solve the Hamiltonian and momentum constraints at initial time for the desired physical system (a complete review about the construction of initial data in General Relativity can be found in [14]). Once the constraints are solved, the evolution equations are used to evolve the so constructed initial data; for instance, in the ADM formulation of General Relativity the dynamical variables to be evolved are the three metric and the extrinsic curvature of the space-like hypersurfaces [7], the constraints are used only to monitor the accuracy of the results.

In the present case the momentum constraint has not been considered for the evolution and the shift has been fixed $\beta^r = 0$, which implies that one has to solve the Hamiltonian constraint and (24) at initial time. Fortunately, these are ODEs that can be solved using standard solvers (see [11] for a revision on such integrators).

Inspection of Eqs. (23) and (24) indicates that one needs to provide values for π and ψ at initial time. This can be achieved by supplying the initial profile for ϕ and -as done for the wave equation- assume time symmetry at initial time, which implies $\pi = 0$. As before, one chooses a gaussian profile, this time centered at the origin of the coordinates, *i.e.* $\phi(0,r) = Ae^{-r^2/\sigma^2}$, and its spatial derivative is $\psi(0,r)$. It could be any other profile, but having a zero function near the boundaries avoids discontinuities at the edge of the numerical domain.

The construction of the initial data works as follows:

i) input ϕ,

ii) calculate its spatial derivative ψ,

iii) assume $\pi = 0$,

iv) integrate the Hamiltonian constraint (23) assuming spatial flatness at the origin ($a = 1$) up to the outer edge of the numerical domain,

v) assume the space-time is Schwarzschild-like at the edge of the numerical domain, thus assume $\alpha(0, r_N) = 1/a(0, r_N)$ and integrate the slicing condition (24) for α inwards.

The integration of the lapse and of the Hamiltonian constraint is done with an ODE integrator that uses finite differencing, like a Runge-Kutta algorithm of second or fourth order that can be constructed from scratch (see *e.g.* Ref. 11).

4.2. Evolution

As for the case of the wave equation, centered finite differencing is used and the domain is discretized in the same manner as for the wave equation. The system of equations to be solved is (23,24) and (26-28). The first two equations are ODEs in r and the other three are partial evolution equations. Therefore, the last three equations drive the evolution of the initial data, and therefore the value of the stress-energy tensor; the other two equations are Einstein's equations that are to be solved once there are new values for the scalar field and its derivatives [π and ψ, see (20) and (23)] have been obtained.

The procedure is as follows:

i) take the initial data constructed in the previous subsection,

ii) evolve this data using (26-28),

iii) apply boundary conditions to the scalar field and its derivatives,

iv) solve the Hamiltonian constraint (23) outwards assuming spatial flatness at the origin $a(r_0) = 1$,

v) at the outer boundary assume the space-time is Schwarzschild like and define $\alpha(r_N) = 1/a(r_N)$, then integrate the slicing condition inwards up to the origin,

vi) use the new values of α and a to calculate new values for the scalar field variables using (26-28), vii) go to (iii).

At each time step, the metric functions α and a are related to each other at the outer boundary imposing the condition $\alpha(r_N) = 1/a(r_N)$, but nothing has been said about the scalar field near the boundaries (point (iii) above). What is assumed here (and could be improved on) is that at the outer edge of the numerical domain the space-time is so flat that the scalar field behaves as a spherical wave function, that is, the relation

$$\psi = -\pi - \phi/r \tag{29}$$

holds, which is a relation that involves the information of the metric functions too ($\pi = a\partial_t\phi/\alpha$). However, not all the information needed is available: according to Eq. (26) the scalar field can be integrated up to the boundary because the right hand side does not contain spatial derivatives and there is no need to apply a condition on ϕ; given that π is the time derivative of the field one can assume it satisfies the equation of a spherical wave too, that is, it is a solution of the equation:

$$\partial_r\pi + \partial_t\pi + \pi/r = 0. \tag{30}$$

In order to find a solution to this equation, the one sided operators defined in Sec. 2.1. are useful to calculate the spatial derivative needed in Eq. (30), because in order to calculate $\partial_r\pi$ only points within the domain are used, including $\pi(r_N)$; also the time derivative contains $\pi(r_N)$ at the current time; the rest is solving for this value in the discretized version of (30). Once $\pi(r_N)$ is known, one uses (29) to calculate $\psi(r_N)$ and the boundary problem is solved.

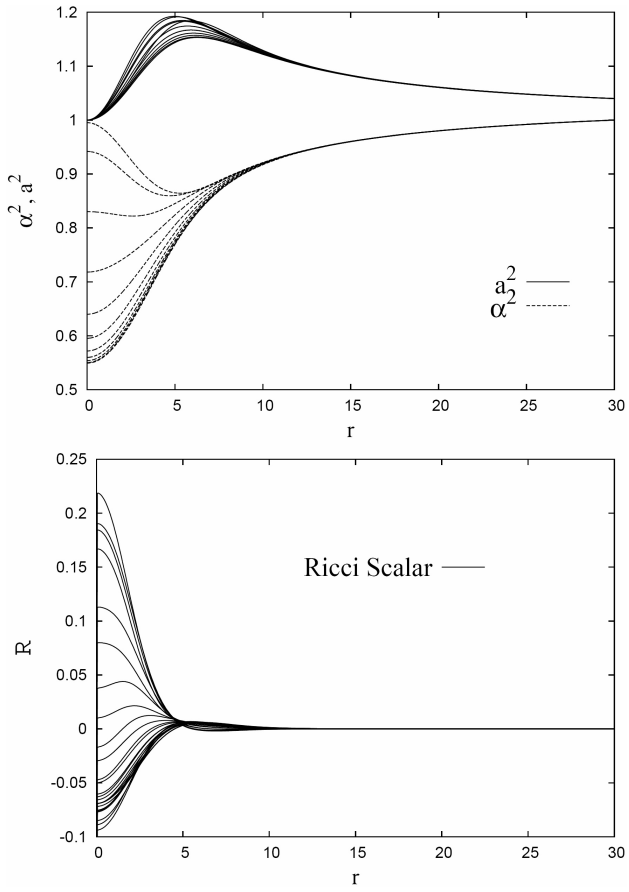

FIGURE 5. (Top) Snapshots of the metric functions a^2 and α^2. (Bottom) Snapshots of the Ricci Scalar R are shown; perhaps this might be one of the simplest solution which has a time-dependent geometry.

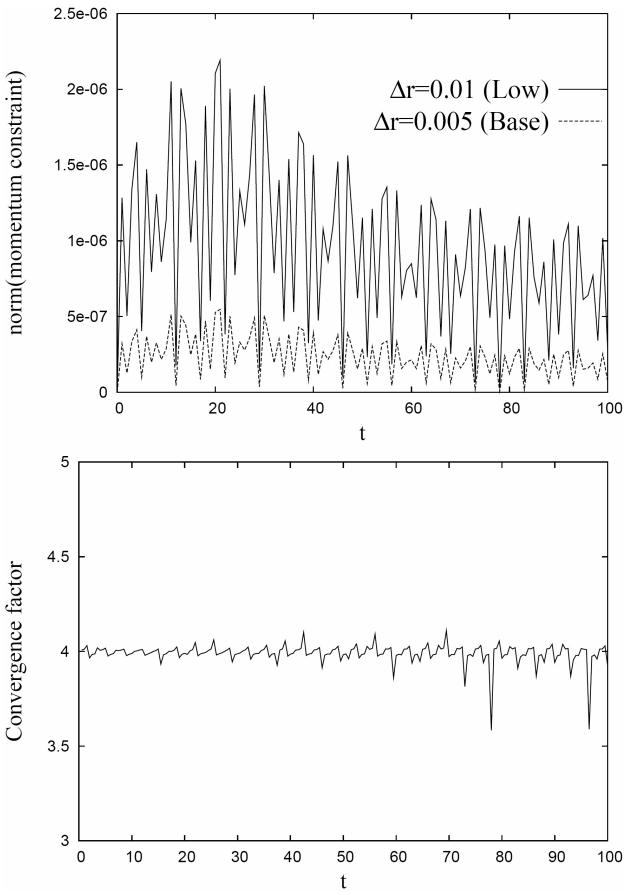

FIGURE 6. (Top) The root mean square norm (it could be any other norm and the qualitative behavior would be the same) of the momentum constraint for two simulations using different resolutions is shown. (Bottom) The convergence factor as defined in (4) is shown for the resolutions used. The fact that the value of the constraint using the base resolution is four times smaller than that obtained with the coarse resolution indicates second order convergence to the value zero, which indicates that in the continuum limit (25) is satisfied and that the Δt and Δr used for these simulations are in the convergence regime (see Sec. 2.2.). The convergence factor departs from the value 4 at certain moments, which indicates that there is a phase shift of the quantity we calculate (the momentum constraint in this case) between one resolution and the other.

In order to illustrate that these algorithms work, it suffices to follow the recipe above with $A = 0.3$ and $\sigma = 5.35$. Any other parameters could have been chosen, and this ones were used because they result in a long lived non-trivial oscillating solution. The boundary was chosen at the location $r_N = 30$ so that the matter was pretty well localized near the origin. In Fig. 5 the dynamical behavior of the metric functions is shown; in fact the solution appears to be a long lived solution. The Ricci scalar is also shown which indicates the dynamical behavior of the geometry of this space-time. A Fourier transform of the central value of this quantity reveals a quasinormal low frequency mode and high frequency modes that correspond to overtones of the oscillation of the scalar field [12].

One cannot be sure that the solution calculated corresponds to a solutions of Einstein's equations until verifying the momentum constraint (25). Although at the continuum limit this equation must be satisfied provided the code is stable, one has to verify that the discretization error converges to zero. This equation has not been used to evolve the system and one is not aware of its validity. In Fig. 6 the value of the quantity $\partial_t a - (1/2)r\alpha\phi\pi$ is presented for the long lived configuration illustrated here; in theory -and in the continuum limit- such quantity should be zero. However what is shown here is that in the continuum limit it actually converges to zero.

Another illustrative situation occurs with $A = 0.4$ and $\sigma = 5.35$. In such case the object is compact enough to collapse into a black hole. In Fig. 7 snapshots of the lapse are shown; after a few oscillations the configuration finally collapses. The coordinates used here are not the most adequate to continue the evolution of the black hole accurately, for which penetrating coordinates are required (see [30] for an example on how to use such coordinates and a non-zero shift for a quite similar physical system).

4.3. Epilogue of real scalar fields: oscillatons

Other applications of the algorithms described above, include the study of the critical phenomena as done in the classical paper by Choptuik [15].

Furthermore, I would like to highlight the interesting case of long lived solutions called oscillatons. These oscillatons are the solutions to the initial value problem by assuming that the scalar field and the metric functions can be expressed as a Fourier series. The result is that like other type of stars (neutron stars or boson stars below) the equilibrium configurations constructed under the Fourier series assumption, show stable and unstable branches; that is, stable configurations are long lived and unstable configurations collapse into black holes. The first reference to oscillatons is Ref. 16; a recent and detailed analysis of oscillatons can be found in Ref. 12; an astrophysical application of oscillatons related to dark matter appears in Ref. 13.

5. Self-gravitating complex scalar field: the boson star case

5.1. The system of equations

A generalization of the former case is the complex scalar field system, in which a complex scalar field $\phi = \phi_1 + i\phi_2$ provides the matter source in Einstein's equations. The stress-energy tensor in this case is:

$$T_{\mu\nu} = \frac{1}{2}[\partial_\mu\phi^*\partial_\nu\phi + \partial_\mu\phi\partial_\nu\phi^*] - \frac{1}{2}g_{\mu\nu}[\phi^{*,\alpha}\phi_{,\alpha} - V(|\phi|^2)], \qquad (31)$$

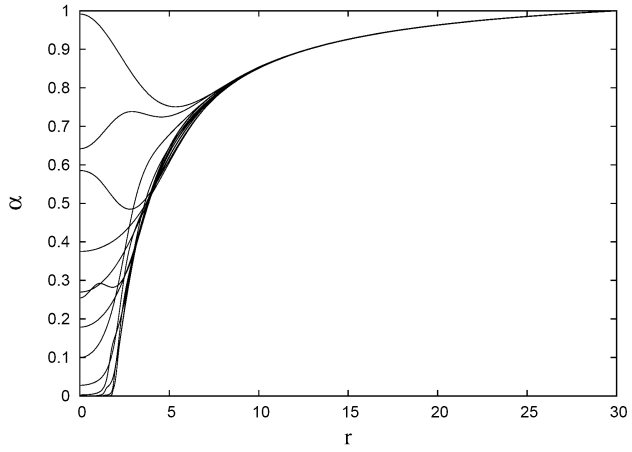

FIGURE 7. Snapshots of the lapse for a configuration that collapses into a black hole. After a few oscillation the lapse finally collapses, which indicates -in the coordinates used- the formation of an apparent horizon.

where $V(|\phi|^2)$ is the potential of self-interaction and the star stands for complex conjugate; in these notes only the case

$$V = \frac{1}{2}m^2|\phi|^2 + \frac{\lambda}{4}|\phi|^4$$

is considered, where again m is usually understood as the mass of a boson and λ is the coefficient of a two body self-interaction mean field approximation. The Klein-Gordon equation is again

$$\left(\Box - \frac{dV}{d|\phi|^2}\right)\phi = 0 \tag{32}$$

where as before

$$\Box\phi = \frac{1}{\sqrt{-g}}\partial_\mu[\sqrt{-g}g^{\mu\nu}\partial_\nu\phi].$$

Notice that this equation is a generalization of (22) for an arbitrary potential. Again g and $g^{\mu\nu}$ are the geometric quantities of the space-time. Considering the real and imaginary parts of the field, the KG equation can be written as two equations:

$$\left(\Box - \frac{dV}{d|\phi|^2}\right)\phi_1 = 0, \quad \left(\Box - \frac{dV}{d|\phi|^2}\right)\phi_2 = 0. \tag{33}$$

The equations for the metric functions a and α are needed to complete the set of equations that describes the system; the line element assumed is again (21). As in the previous case, it is convenient to define first order variables, which this time are $\pi_i = (a/\alpha)\partial_t\phi_i$ and $\psi_i = \partial_r\phi_i$, for each $i = 1, 2$. With these new variables the KG system is translated into the set

$$\begin{aligned}
\partial_t\phi_1 &= \frac{\alpha}{a}\pi_1, \\
\partial_t\phi_2 &= \frac{\alpha}{a}\pi_2, \\
\partial_t\psi_1 &= \partial_r\left(\frac{\alpha}{a}\pi_1\right), \\
\partial_t\psi_2 &= \partial_r\left(\frac{\alpha}{a}\pi_2\right), \\
\partial_t\pi_1 &= \frac{1}{r^2}\partial_r\left(r^2\frac{\alpha}{a}\psi_1\right) - \frac{1}{2}a\alpha\frac{dV}{d|\phi|^2}\phi_1, \\
\partial_t\pi_2 &= \frac{1}{r^2}\partial_r\left(r^2\frac{\alpha}{a}\psi_2\right) - \frac{1}{2}a\alpha\frac{dV}{d|\phi|^2}\phi_2.
\end{aligned} \tag{34}$$

Einstein's equations coupled to a complex scalar field, for the line element (21) and the variables defined above are very similar to those of the real scalar field case:

$$\begin{aligned}
\frac{\partial_r a}{a} &= \frac{1-a^2}{2r} + \frac{\kappa_0 r}{4}[\pi_1^2 + \pi_2^2 + \phi_1^2 \\
&\quad + \phi_2^2 + a^2 V]
\end{aligned} \tag{35}$$

$$\frac{\partial_r\alpha}{\alpha} = \frac{a^2-1}{r} + \frac{a'}{a} - \frac{\kappa_0 r a^2}{2}V \tag{36}$$

$$\partial_t a = \frac{\kappa_0 a r}{2}[\partial_r\phi_1\partial_t\phi_1 + \partial_r\phi_2\partial_t\phi_2] \tag{37}$$

These equations correspond to the Hamiltonian constraint, the slicing condition and to the rt component of the Einstein's equations (the momentum constraint) respectively. Clearly, this set of equations is overdetermined again, and it is necessary to choose two of these three equations to be solved; as before, the momentum constraint (37) is not solved during the evolution, but used only for monitoring the accuracy of the numerical calculations.

5.2. Initial data for Boson Stars and the test

Boson stars (BSs) are solutions to the above set of equations under a particular condition: the scalar field is harmonic in time $\phi(r,t) = \phi_0(r)e^{-i\omega t}$. This condition implies that the stress energy tensor in (31) is time-independent, which implies through Einstein's equations that the geometry is also time-independent. That is, there is a time-dependent scalar field oscillating upon a time-independent geometry whose source is the scalar field itself. It is possible to construct boson stars solutions assuming that the metric can be written in Schwarzschild coordinates as

$$ds^2 = -\alpha(r)^2dt^2 + a(r)^2dr^2 + r^2d\Omega^2.$$

Under these conditions the Einstein-Klein-Gordon system of equations reads:

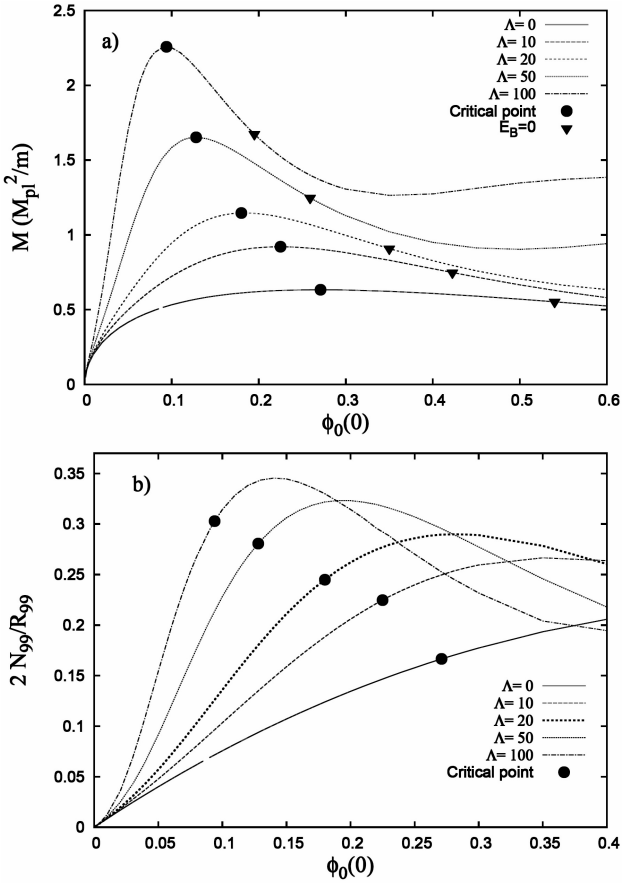

FIGURE 8. (a) Sequences of equilibrium configurations for different values of Λ are shown as a function of the central value of the scalar field $\phi_0(0)$; each point in the curves corresponds to a solution of the eigenvalue problem and represents a boson star configuration. The filled circles indicate the critical solution that divides the stable from the unstable solutions. The inverted triangles indicate the point at which the binding energy is zero. Those configurations between the circles and the triangles (along each sequence) collapse into black holes even for infinitesimal perturbations (see [22] for the tracking of the formation of an event horizon out of an unstable boson star). Configurations to the right of the triangles disperse away. (b) The compactness of each solution is shown. The critical point is also marked.

$$\frac{\partial_r a}{a} = \frac{1-a^2}{2r} + \frac{1}{4}\kappa_0 r \times \left[\omega^2\phi_0^2\frac{a^2}{\alpha^2} + (\partial_r\phi_0)^2 + a^2(m^2\phi_0^2 + \frac{1}{2}\lambda a^2\phi_0^4)\right],$$

$$\frac{\partial_r \alpha}{\alpha} = \frac{a^2-1}{r} + \frac{\partial_r a}{a} - \frac{1}{2}\kappa_0 r a^2\phi_0^2(m^2 + \frac{1}{2}\lambda\phi_0^2),$$

$$\partial_{rr}\phi_0 + \partial_r\phi_0\left(\frac{2}{r} + \frac{\partial_r\alpha}{\alpha} - \frac{\partial_r a}{a}\right) + \omega^2\phi_0\frac{a^2}{\alpha^2} - a^2(m^2+\lambda\phi_0^2)\phi_0 = 0. \quad (38)$$

The system (38) is a set of coupled ordinary differential equations to be solved under the conditions of spatial flatness at the origin $a(0) = 1$, $\phi_0(0)$ finite and $\partial_r\phi_0(0) = 0$ in order to guarantee regularity and spatial flatness at the origin, and $\phi_0(\infty) = \phi_0\prime(\infty) = 0$ in order to ensure asymptotic flatness at infinity as described in Refs. 17 to 21; these conditions reduce the system (38) to an eigenvalue problem for ω. The solution is calculated numerically using finite differencing with an ordinary integrator (fourth order Runge-Kutta algorithm) and a shooting routine that bisects the value of ω.

In order to recover the evolution equations without the physical parameters m, λ and ω (remember, m and λ are parameters of the scalar field potential), it suffices to perform the following rescaling of the equations:

$$\phi_0 \to \sqrt{\kappa_0/2}\phi_0, \qquad r \to mr,$$
$$t \to \omega t, \alpha \to \frac{m}{\omega}\alpha \qquad \text{and} \qquad \Lambda = \frac{2\lambda}{\kappa_0 m^2}.$$

The result is that the physical parameters vanish from the equations and that the radial coordinate has units of m and the time has units of ω. In these new units the initial data for boson stars are used to start the evolution of the system through the equations (34)-(37).

Before showing the evolution of boson stars let us gain some intuition about the boson star solutions constructed. The solutions of (38) define sequences of equilibrium configurations like those shown in Fig. 8a. In the curves two important points for each value of Λ are marked:

i) the critical point -marked with a filled circle- indicating the threshold between the stable and unstable branches of each sequence, that is, configurations to the left of this point are stable and those to the right are unstable as found through the analysis of perturbations [20, 21], catastrophe theory [23] and full non-linear evolution of the equilibrium solutions [18, 19, 22] and

ii) the point at which the binding energy $E_B = M - Nm = 0$ marked with an inverted filled triangle, where

$$N = \int j^0 d^3x = \int \frac{i}{2}\sqrt{-g}g^{\mu\nu}[\phi^*\partial_\nu\phi - \phi\partial_\nu\phi^*]d^3x$$

is the number of particles and $M = (1-1/a^2)r/2$ evaluated at the outermost point of the numerical domain is the Schwarzschild mass; the configurations between the instability threshold and the zero binding energy point collapse into black holes whereas those to the right disperse away as shown in Ref. 22. The units for M and N are given in M_{pl}^2/m, where M_{pl} is the Planck mass and m is the mass of the boson.

Because the mass of the configurations in Fig. 8(a) scales with m, the original use of the self-interaction Λ was to allow bigger masses even if the mass parameter m was fixed [24] and thus BS configurations seemed to be similar to compact objects like neutron stars [24]. In Fig. 8b the compactness of equilibrium configurations is shown. Provided BSs have no

defined surface one considers that the radius containing 99% (R_{99}) of the total particle number (following [18, 19] where 95% was considered instead) is a reasonable place where to measure the gravitational field of the star; thus the compactness plotted in Fig. 8b is defined as $2N_{99}/R_{99}$, where N_{99} is the number of particles integrated up to R_{99}. For big values of Λ it is possible to construct compact stars that can play the role of astrophysical compact objects (see Ref. 24).

5.3. The evolution of boson stars

The illustrative situation in this case is the test of the hypotheses (harmonic time dependence of the scalar field and time independence of the metric functions). Let us see whether this is true when using the system of equations (34)-(36) to evolve boson star initial data. What is needed is to set up the initial data calculated from (38) and use them as initial data for the evolution system (34)-(36). The procedure to carry out the evolution of the system is the same as the one used to evolve the real scalar field in the previous section. In fact, in the present case the boundary conditions on the metric functions are exactly the same as in the previous section, and the boundary conditions for the scalar field are as follows: the condition over π_i is the same as (30) and the condition over ψ_i is (29) for each $i = 1, 2$. That is, the real and imaginary parts of the scalar field are considered to behave as outgoing spherical waves separately, which is reasonable because the equations for ϕ_1 and ϕ_2 are decoupled [see Eq. (33)].

5.4. Stable Boson star

As an example, the configuration with values $\phi_0(0) = 0.2$, $\Lambda = 0$, with $M = 0.6208(M_{pl}/m)$ is analyzed. The corresponding configuration is located near the critical point on the sable branch of the $\Lambda = 0$ curve in Fig. 8(a). In Fig. 9 the maximum of the metric function a in time is shown for this case. What can be seen is that the result is not as strict as the assumptions made about the time-independence of the metric. Instead, this metric function oscillates in time (it is not time-independent). However, what is also shown in that plot is that the numerical calculations converge to the time-independent result with second order, according to the results presented in Sec. 2.2 using two resolutions and assuming that the calculation of the maximum of a from the solution of the eigenvalue problem is the exact solution.

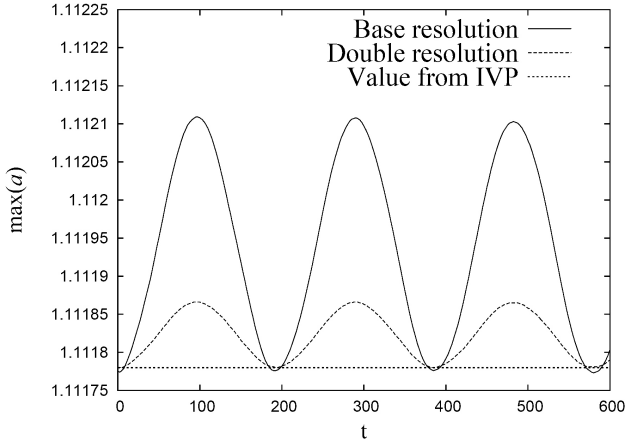

FIGURE 9. The maximum value of a in time for a BS with $\phi_0(0) = 0.2$ and $\Lambda = 0$. According to the assumptions made during the construction of equilibrium configurations this function should be time-independent. However, this function is shown for two different resolutions $\Delta r = 0.05, 0.025$. The value of $max(a)$ calculated from the initial value problem $max(a_{ivp}) = 1.11178$ is also shown. The fact that the plot with the coarse resolution is four times bigger with respect to the constant line 1.11178 indicates that it converges to such value with second order (see Sec. 2.2).

Aside of showing that in the continuum limit the metric (*e.g.* a) is time independent, the test of fire consists in showing that the scalar field is truly oscillating meanwhile. In Fig. 10 the central value of ϕ_1 is shown. A Fourier Transform reveals that the fundamental frequency of oscillation of this field corresponds to the eigenvalue calculated when solving the initial value problem (in the units used here, where $t \to \omega t$, the frequency is $\omega = 1/2\pi$).

Next, there is an issue with the momentum constraint that was not solved. Not shown here, but convergence to zero of the expression $\partial_t a - (ar/2)[\partial_r\phi_1\partial_t\phi_1 + \partial_r\phi_2\partial_t\phi_2]$ is achieved with second order, the same case as that sown in Fig. 6 for the real scalar field case.

Finally, in order to show the difference between this solution and that of the real scalar field, in Fig. 11 snapshots of the metric functions are shown. The time-dependence of the solution is as small as shown in Fig. 9. The metric is truly nearly time-independent for all the values of r. In a way, the real and imaginary parts of ϕ conspire to drive the system in such a way that the geometry does not *feel* the dynamics of the scalar field.

5.5. Unstable Boson Star

In order to show how a black hole forms, an initial configuration that belongs to the unstable branch is chosen. The discretization error suffices to act as a perturbation that triggers the collapse of the configuration. For this purpose consider the configuration with $\phi_0(0) = 0.25$ and $\Lambda = 10$ (which can be seen to be unstable from Fig. 8a). The results of the evolution are summarized in Fig. 12, where snapshots of the lapse are shown; in fact the lapse collapses to zero in a region expected to be covered by a horizon. In the coordinates used, an apparent horizon has been formed when the lapse is sufficiently near zero. However, it is simple to use different coordinates allowing one to calculate the location, mass and possible oscillations of an apparent horizon. The whole process where even the event horizon was calculated during the collapse of an unstable BS can be found in Ref. 22. However, at this point the results in this section correspond to the typical results found for spherically symmetric BSs in the canonical papers [18, 19].

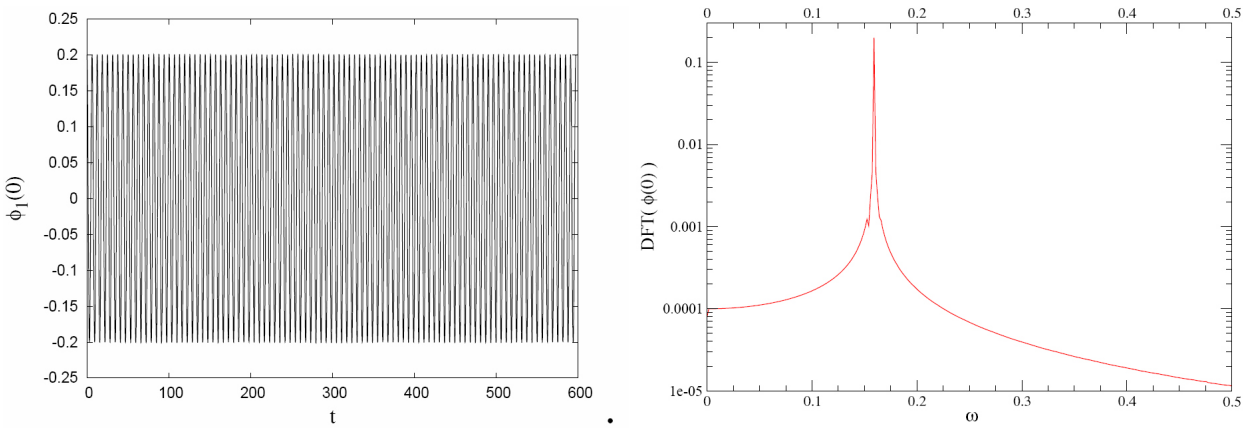

FIGURE 10. (Left) The central value of ϕ_1 versus time for a BS with $\phi_0(0) = 0.2$ and $\Lambda = 0$. (Right) The Fourier Transform of the central value of the field. The peak shows up at $\omega = 1/2\pi$.

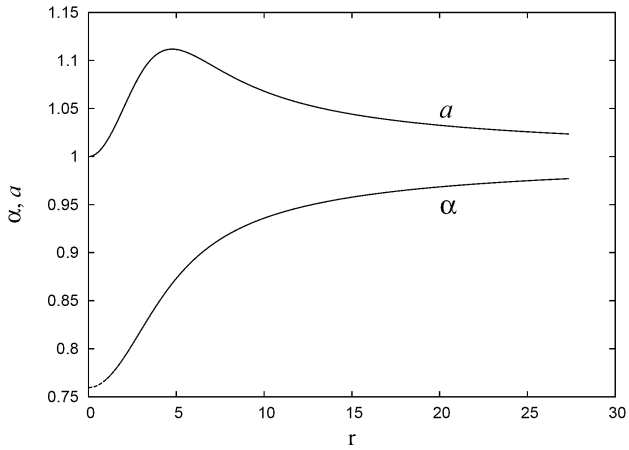

FIGURE 11. Snapshots at several times of the metric functions are shown. The nearly time-independence is manifest over the whole spatial domain, not only near the region of the maximum of a.

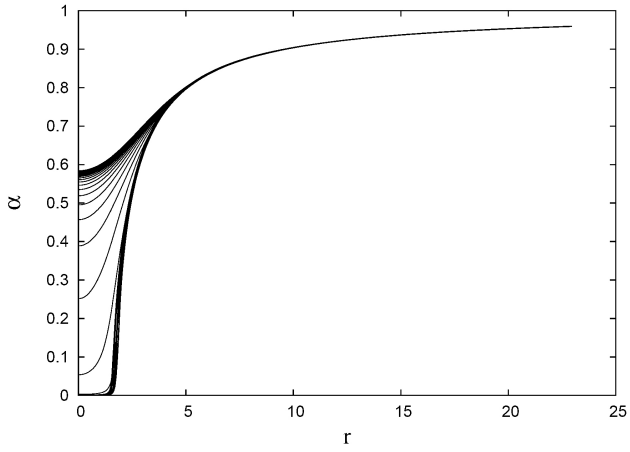

FIGURE 12. Snapshots of the lapse function for a BS with $\phi_0(0) = 0.25$ and $\Lambda = 10$. After a period of doubt, the lapse finally collapses to zero, which indicates that a horizon has been formed. A plot of the energy-density reveals a divergence at the origin; the geometric invariants also show a divergence.

5.6. Epilogue of Boson Stars

Boson stars are self-gravitating systems that help illustrating how more complicated systems -like neutron stars- evolve. A main property of scalar fields is that the evolution equations are linear in the degenerated part, and no shocks are formed during the evolution. In fact, as seen in the examples presented here, the evolution equation of a scalar field is the wave equation with a more general D'Alambertian.

Boson stars have been studied not only as toy models but have also been considered as potentially existing astrophysical objects. In this sense, BSs can be assumed to potentially exist because they can be considered to represent the final stage of zero temperature self-gravitating Bose Condensates [25], which have regular geometry and smooth matter distribution, with no horizons or singularities. Because these objects do not emit in the electromagnetic spectrum they are dark (or black, in the sense of black holes). In fact, the Newtonian version of BSs have been considered as models of galactic halos explaining the galaxy formation process under the scalar field dark matter hypothesis [25].

There are relevant results that can be obtained with the knowledge found in these notes. For instance, it is possible to infer differences between a Boson Star and a Black Hole (BH) when matter is accreting [26–28]. It is also possible to push forward the ideas in here, so that BSs can be considered to be sources of gravitational waves, which could potentially determine the existence of these objects [29].

6. Final remarks

Throughout these notes it has been shown how to solve PDEs related to general relativity using finite difference approximations. The idea has been to attract the interest of students and researchers working on topics related to gravitation, to get involved in problems with less symmetries than the cases at hand of analytic techniques (recall that the cases seen here are spherically symmetric but time-dependent). Among others,

an attractive advantage of using numerical calculations is related to nonlinear perturbations of gravitating systems: when using numerical relativity there are two steps to carry out, one is to probe that linear perturbation theory is correct by analyzing the resulting quasinormal modes for a given system. The other is that the solution is fully non-linear and therefore other instability modes can be studied during the evolution.

The examples related to the self-gravitating scalar fields can be improved easily. The idea is to write down the equations as done for the wave equation. An example of such free evolution for similar cases of self-gravitating scalar fields with spherical symmetry can be found in [30], where even the gauge is allowed to evolve. This is an example close to the production codes in full three dimensions with no symmetries for hard core problems, where self-correcting gauge conditions are used. Needless to say that scalar fields are everywhere in higher dimensional theories and models, where possibly the assumptions and simple gauge conditions studied here suffice to find interesting results.

An important point related to the algorithms is the fact that in the examples developed here, the resolution in all cases has been uniform. This is enough for the cases studied in these notes, however it does not suffice in other cases, for example, systems in full three dimensions without symmetries, where all the variables depend on three coordinates; in such case, every single function needs N^3 allocated real numbers, whereas in the cases here only N are needed; therefore memory is an important issue and it has to be optimized. In order to do so, two ideas are currently in action, one is the mesh refinement technique, which sets up different resolutions in different regions of the spatial domain, using higher resolution where the geometry is more deformed and a coarse one where the functions are nearly constant; the other is the use of non-uniform discretizations, that is, the spatial grid points are spatially closer to each other in a desired region whereas they could be more separated in other regions; this technique can be applied to the examples above by implementing a logarithmic radial coordinate (for instance), which provides closer nearby points around $r = 0$ and separate points in the far region; the cheap price to pay is that all the functions have to be transformed (some of them as tensors) to the new coordinate system, but the gain is that the boundaries are very far away, which, for highly non-linear problems is an important issue.

Finally, it is worth mentioning that the algorithms can be improved, can be more efficient and able to allow simulations to be carried out on smaller computers. It is also important to remark that there is plenty of problems that are still unsolved within gravitational physics and relativistic astrophysics, which open a wide collection of topics to work on by using the numerical techniques. In order to go deeper into the field of numerical relativity and the problems of the state of the art, the reader is invited to consult the following reviews: [31] about the numerical hydrodynamics in general relativity, [32] about the construction of initial data in numerical relativity, [33] about the numerical hydrodynamics in special relativity, [34] for a review on physical and relativistic numerical cosmology, [35] for a review on numerical relativity and [36] to learn about the status of numerical relativity.

Acknowledgments

This work is partly supported by projects CIC-UMSNH-4.9 and PROMEP-UMICH-PTC-121 and PROMEP-UMSNH-CA-22.

1. M. Campanelli, C.O. Lousto, P. Marronetti, and Y. Zlochower, *Phys. Rev. Lett.* **96** (2006) 111101.
2. J.G. Baker, J. Centrella, Dae-Il Choi, M. Koppitz, and J. van Meter, *Phys. Rev. Lett.* **96** (2006) 111102.
3. M.W. Choptuik *et al.*, *Phys. Rev. D* **68** (2003) 044001.
4. O. Sarbach and L. Lehner, *Phys. Rev. D* **71** (2005) 026002.
5. J. Thornburg, gr-qc/9906022
6. I. Hawke, S. Husa, and B. Szilagyi, http:// numrel.aei.mpg.de/ Education/Tutorials/School04/tov.ps
7. C. Bona and C. Palenzuela-Luque, *Elements of Numerical Relativity, Lect. Notes Phys.* **673** (Springer, Berlin Heidelberg, 2005).
8. P. Diener and F. S. Guzmán, http://numrel.aei.mpg.de/ Education/Tutorials/trackI/tutorial1.pdf
9. B. Gustafsson, H-O. Kreiss, and J. Oliger, *Time Dependent Problems and Difference Methods* (Wiley-Interscience, 1996).
10. R.J. LeVeque, in *Numerical methods for conservation laws* (Birkhauser, Basel 1992).
11. W.H. Press, S.A. Teukolsky, W.T. Watterling, and B.P. Flannery, *Numerical Recipes in Fortran* (Cambridge University Press, 1992).
12. M. Alcubierre *et al.*, *Class. Quantum Grav.* **20** (2003) 2883.
13. M. Alcubierre *et al.*, *Class. Quantum Grav.* **19** (2002) 5017.
14. Gregory B. Cook, Living Reviews in Relativity. 2005-5. http://www.livingreviews.org/Articles/Volume3/2000-5cook
15. M.W. Choptuik, *Phys. Rev. Lett.* **70** (1993) 9.
16. E. Seidel and W-M. Suen, *Phys. Rev. Lett.* **66** (1991) 1659.
17. R. Ruffini and S. Bonazolla, *Phys. Rev.* **187** (1969) 1767.
18. E. Seidel and W-M. Suen, *Phys. Rev. D* **42** (1990) 384.
19. J. Balakrishna, E. Seidel, and W-M. Suen, *Phys. Rev. D* **58** (1998) 104004.
20. M. Gleiser, *Phys. Rev. D* **38** (1988) 2376.
21. S.H. Hawley and M.W. Choptuik, *Phys. Rev. D* **62** (2000) 104024.

22. F.S. Guzmán, *Phys. Rev. D* **70** (2004) 044033.
23. F.E. Schunck and D.F. Torres, *Int. J. Mod. Phys. D* **9** (2000) 601.
24. M. Colpi, S.L. Shapiro, and I. Wasserman, *Phys. Rev. Lett.* **57** (1986) 2485.
25. F.S. Guzmán and L.A. Ureña-López, *ApJ* **645** (2006) 814; astro-ph/0603613.
26. D.F. Torres, S. Capozziello, and G. Lambiase, *Phys. Rev. D* **62** (2000) 104012; F.S Guzman, Phys. Rev. D 73 (2006) 021501(R).
27. D.F. Torres, *Nucl. Phys. B* **26** (2002) 377.
28. Y-F. Tuan, R. Narayan, and M.J. Rees, *ApJ* **606** (2004) 1112.
29. J. Balakrishna, R. Bondarescu, G Daues, F.S. Guzmán, and E. Seidel, *Class. Quantum Grav.* **23** (2006) 2631.
30. M. Alcubierre, J.A. González, and M. Salgado, *Phys. Rev. D* **70** (2004) 064016.
31. J.A. Font, "Numerical Hydrodynamics in General Relativity", Living Rev. Relativity 6, (2003), http://www.livingreviews.org/lrr-2003-4
32. Gregory B. Cook, "Initial Data for Numerical Relativity", Living Rev. Relativity 3, (2000), http://www.livingreviews.org/lrr-2000-5
33. J.M. Martí and E. Müller, "Numerical Hydrodynamics in Special Relativity", Living Rev. Relativity 6, (2003), http://www.livingreviews.org/lrr-2003-7
34. Peter Anninos, "Computational Cosmology: from the Early Universe to the Large Scale Structure", Living Rev. Relativity 1, (1998), http://www.livingreviews.org/lrr-1998-2
35. L. Lehner, *Class. Quant. Grav.* **18** (2001) R25.
36. M. Alcubierre; gr-qc/0412019.